Anharmonicity and the IR emission spectrum of neutral interstellar PAH molecules

Mackie, C.J.; Candian, A.; Lee, T.J.; Tielens, A.G.G.M.

THE JOURNAL OF PHYSICAL CHEMISTRY A
A JOURNAL OF THE AMERICAN CHEMICAL SOCIETY

pubs.acs.org/JPCA

Article

Anharmonicity and the IR Emission Spectrum of Neutral Interstellar PAH Molecules

Published as part of The Journal of Physical Chemistry virtual special issue "10 Years of the ACS PHYS Astrochemistry Subdivision".

Cameron J. Mackie,* Alessandra Candian, Timothy J. Lee, and Alexander G. G. M. Tielens

Cite This: *J. Phys. Chem. A* 2022, 126, 3198–3209

Read Online

ACCESS | Metrics & More | Article Recommendations

ABSTRACT: The characteristics of the CH stretching and out-of-plane bending modes in polycyclic aromatic hydrocarbon molecules are investigated using anharmonic density functional theory (DFT) coupled to a vibrational second-order perturbation treatment taking resonance effects into account. The results are used to calculate the infrared emission spectrum of vibrationally excited species in the collision-less environment of interstellar space. This model follows the energy cascade as the molecules relax after the absorption of a UV photon in order to calculate the detailed profiles of the infrared bands. The results are validated against elegant laboratory spectra of polycyclic aromatic hydrocarbon absorption and emission spectra obtained in molecular beams. The factors which influence the peak position, spectral detail, and relative strength of the CH stretching and out-of-plane bending modes are investigated, and detailed profiles for these modes are derived. These are compared to observations of astronomical objects in space, and the implications for our understanding of the characteristics of the molecular inventory of space are assessed.

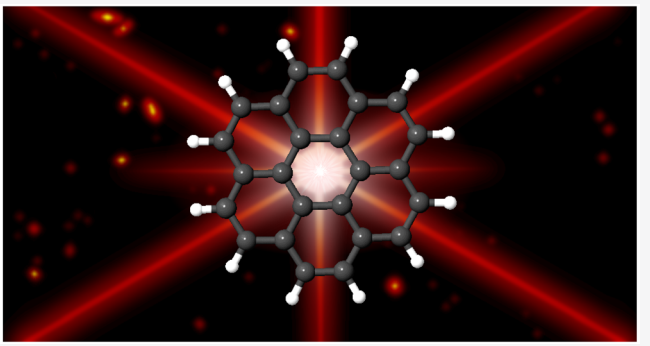

1. INTRODUCTION

The infrared (IR) spectra of many gaseous regions of interstellar space are dominated by strong emission bands at 3.3, 6.2, 7.7, 8.6, 11.2, and 12.7 μm, accompanied by a host of weaker features (cf., ref 1 and references therein). The measured peak positions are very characteristic of aromatic species, and as such these bands are commonly known as the aromatic infrared bands (AIBs). Because these bands are bright, even far from the illuminating stars where the radiative equilibrium temperatures would prohibit dust emission at mid-IR wavelengths, the emission must represent a fluorescence process where absorbed stellar UV photons electronically excite a molecular species that then relaxes through vibrational emission at mid-IR wavelengths.

This general framework is well accepted in the community,[1] and the community has turned toward interpreting the observed spectra in terms of the characteristics of the emitting carriers and relating those to the physical conditions of the medium (e.g., density, temperature, and stellar radiation field). This is often based on fitting the observed spectra with a set of molecular spectra collected in databases. These spectra are calculated using density functional theory (DFT) at zero Kelvin and are corrected for anharmonic effects using frequency scaling factors. Scaling factors are determined by comparing calculated transition frequencies for a set of small PAHs with those measured using matrix isolation spectroscopy (MIS).[2] In recent years, this approach has been further refined by introducing frequency-dependent scaling factors.[3] However, MIS is prone to introducing changes in line positions, intensities, and band profiles of the recorded spectra and even band splittings due to interactions with the matrix environment. Therefore, MIS techniques have a limited accuracy (± 6 cm^{-1}).[4] These theoretical absorption spectra are then converted into emission spectra using simple emission models.[3,5−7] The validity of this procedure is not well established because during radiative vibrational relaxation the anharmonicity and resonances (i.e., nearly degenerate intermode perturbations) can have profound effects on the peak position and profiles of the molecular vibrational modes. Recent experimental[8−11] and quantum chemical[12−14] studies have focused on quantifying these effects

Received: March 16, 2022
Revised: April 26, 2022
Published: May 11, 2022

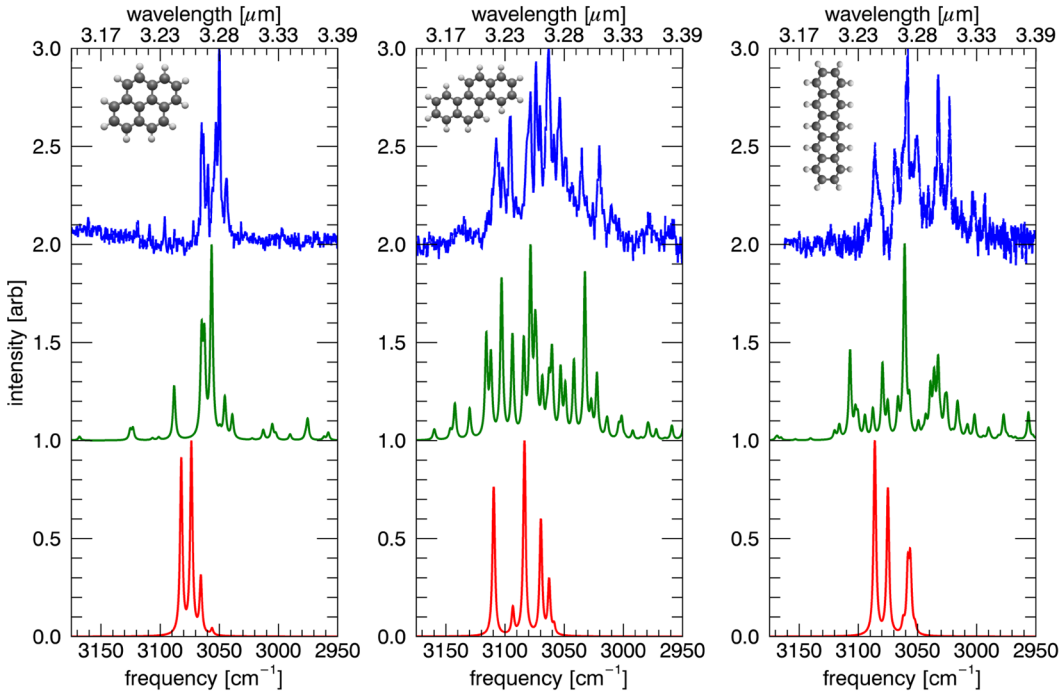

Figure 1. Absorption spectra of pyrene (left), chrysene (middle), and pentacene (right) in the 3 μm CH stretching region. (Top) Gas-phase absorption spectra measured using an ion-dip technique. (Middle) Computed absorption spectra accounting for anharmonicity and resonance effects. (Bottom) Computed absorption spectra in the double-harmonic approximation, with frequencies scaled by a factor of 0.963.[9,13]

on the absorption spectra, and sophisticated simulations have been developed to incorporate them into emission models.[15−18]

In this article, we apply these newly developed models in order to study the emission characteristics of the CH stretching and bending modes of neutral polycyclic aromatic hydrocarbons (PAHs). The emission model is briefly summarized in section 2. Section 2.2 compares the experimental spectra of these modes with quantum chemical calculations to validate the quantum chemical results and assess the reliability of the spectra collected in databases. Emphasis is placed on the effects of anharmonicity on the emission profiles. The astrophysical implications are presented in section 4. Finally, the results are summarized in section 5.

2. METHODS

2.1. Emission Model. The details of the simulated PAH cascade emission model have been described in detail previously.[12,18,19] A second-order vibrational perturbation treatment (VPT2) is applied to the harmonic vibrational modes of the PAHs in order to obtain the anharmonic constants, x (see ref 20 for their derivation), which in turn are used to calculate the perturbed vibrational energies of mode ν given by

$$E(\nu) = \sum_k \omega_k\left(n_k + \frac{1}{2}\right) + \sum_{k\le l} x_{kl}\left(n_k + \frac{1}{2}\right) \times \left(n_l + \frac{1}{2}\right) \quad (1)$$

where ω represents the harmonic frequencies, and n represents the number of quanta in the vibrational modes. Equation 1 is valid for an asymmetric top.

Transition energies between adjacent vibrational levels of a given mode are then given by

$$\Delta E'^{(k)}(\{n\}) = \omega_k + 2x_{kk}(n_k) + \frac{1}{2}\sum_{i\neq k} x_{ik} + \sum_{i\neq k} x_{ik}n_i \quad (2)$$

where n_k is relative to the upper state and n_i represents a "spectator" mode that is populated but is not involved in the transition.

A Wang−Landau walk[21] is performed over these states for a given energy range (0−8 eV in this work) by randomly increasing or decreasing the vibrational quanta with a given acceptance rate. See refs 16 and 17 for a complete description. This produces energy-dependent spectra for each PAH, which in turn is used to simulate the cascade emission process.

During the cascade emission simulation, the probability of emitting an IR photon at a given energy is proportional to the Einstein A coefficient at that frequency, which is proportional to the calculated intensity (km/mol) of the spectrum at said frequency multiplied by the frequency squared. After recording the emitted IR photon in a histogram of frequencies, the total internal energy is decreased by the energy equal to the emitted IR photon, and the next IR photon is likewise chosen from the appropriate spectrum of the current total internal energy. This process is continued until the PAH has cooled fully. The whole process is then repeated from the initial cascade energy until the desired resolution is obtained.

All parameters for the Wang−Landau walk and the emission model used in this work follow the methods laid out in previous work.[16,17] The geometry optimizations, harmonic calculations, and quartic force field were calculated using the Gaussian 16 software package[22] with density functional theory with the B3LYP[23,24]/N07D[25] functional/basis set combination. The VPT2 treatment was used with SPECTRO,[26] which allowed for the redistribution of intensities over the blocks of mutually resonant modes, the so-called polyads.[17,27]

https://doi.org/10.1021/acs.jpca.2c01849
J. Phys. Chem. A 2022, 126, 3198−3209

A modest rotational broadening of a HWHM of 2 cm^{-1} is applied to all emission spectra in this work in order to soften the sharp zero Kelvin emission edge which occurs prominently at the blue edge of the emission features below 1500 cm^{-1}.[18] This amount of rotational broadening is appropriate for isolated PAHs excited by UV absorption and relaxed through vibrational emission.

2.2. Experimental Validation of the Model. *2.2.1. Laboratory Absorption Spectrum of the CH Stretching Modes.* The aromatic CH stretching modes occur in the 2900−3200 cm^{-1} range, which is broadened a bit from the aromatic CH stretching range in benzene, for example, by Fermi resonances. The use of IR-UV double resonance laser spectroscopic techniques coupled with mass-resolved ion detection has provided high-resolution (1 cm^{-1}) spectra of mass- and conformation-selected PAHs seeded in molecular beams. In combination with anharmonic DFT calculations, the work has provided much insight into the spectral signature of PAHs in this frequency range.[8−10,12−14]

Figure 1 compares the experimental spectra of pyrene, chrysene, and pentacene in the CH stretching region with the computed spectrum in both the harmonic and anharmonic approximations. Harmonic spectra (bottom traces) have been shifted using a scaling factor of 0.963 in order to account for anharmonicity and basis set errors.[2] As Figure 1 illustrates, applying this correction factor results in good agreement in peak position between the computed and the gaseous absorption spectra but misses many new peaks that occur because of resonances.

Figure 1 also compares the ion-dip spectrum with the theoretical spectra computed in the anharmonic approximation (middle trace). This anharmonic approximation also accounts for resonance effects. In this case, no scaling factor has to be applied to obtain good agreement in peak position. In addition, the computed spectra agree reasonably well with the measured spectra when considering the absorption band pattern, the relative intensity, and the frequency range over which absorption occurs. For each species, the difference in absorption activity between the two computed spectra illustrates the importance of resonance interactions, which cannot be accounted for in the harmonic approach.

By comparing the spectra of the three species in Figure 1, we recognize that the symmetric, compact PAH (i.e., pyrene) exhibits IR activity over a much narrower frequency range than do noncompact PAHs. The presence of bay regions (edges containing two bound carbon atoms, which in turn are not bound to any hydrogen atoms) in the molecular structure of chrysene widens the IR activity to a larger frequency range. This shift results from steric hindrance between hydrogens across the bay regions.[28,29] Hence, the spectral activity in the CH stretching region provides direct insight into the structure and symmetry of the emitting molecules.

2.2.2. Laboratory Emission Spectrum of the CH Stretching Modes. Figure 2 compares the calculated emission spectrum of naphthalene with the laboratory spectrum in the CH stretching region. This emission spectrum was measured by the Saykally group[30] using the single-photon infrared-emission spectrometer (SPIRES) interfaced to a vacuum chamber where a pulsed nozzle created a free jet expansion of naphthalene in argon. Seeding occurred by pushing the argon beam through a naphthalene sample reservoir. An excimer laser was used to UV pump the PAH at either 193 or 248 nm, corresponding to 6.4 and 5 eV, respectively. Electronic excitation is quickly followed by internal conversion to the vibrational manifold of

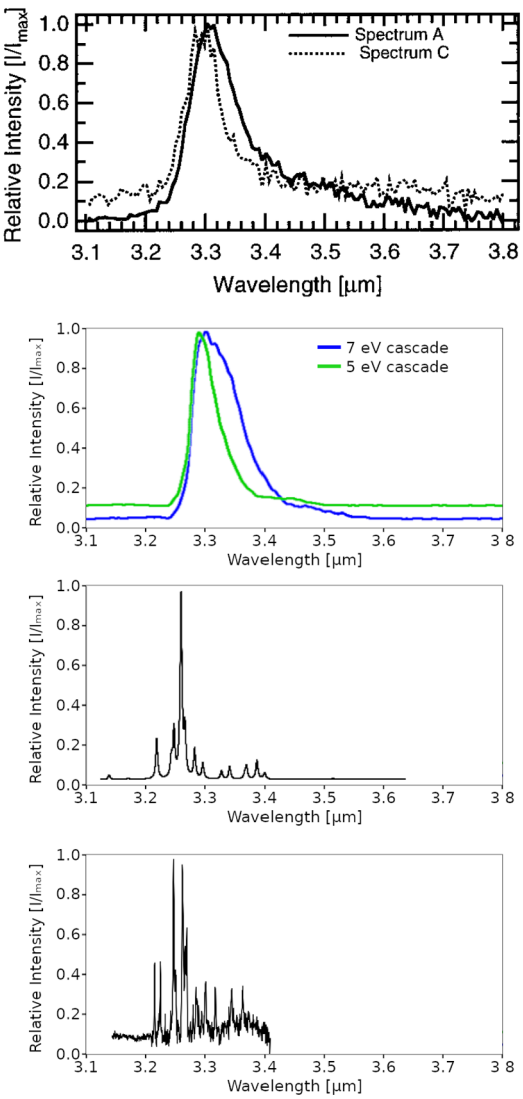

Figure 2. (First panel) Experimentally obtained emission spectra of gas-phase naphthalene, adapted from ref 30. Spectrum A is obtained from a 193 nm laser pulse, and spectrum C is obtained from a 248 nm laser pulse. (Second panel) Theoretical simulation of the top panel using the method described in this article. (Third panel) Measured 30 K absorption spectrum of gas-phase naphthalene using an ion-dip technique.[8] (Fourth panel) Anharmonic spectrum calculated[12] using Gaussian and Spectro (cf., section 2).

lower-lying electronic states, reaching the ground state after about 1 ns.[31−33] However, it should be noted that some species may decay through electronic fluorescence with a quantum yield in the gas phase ranging from 0.1 to 0.45[34] or after crossing over to the triplet state through phosphorescence with a quantum yield of ≃0.02 at low temperatures.[35] The highly vibrationally excited species will relax through the emission of infrared vibrational transitions, and full relaxation will take ≃0.1s. The IR emission spectrum of naphthalene was measured after ≃40 μs, and at that point, the emitting molecule will attain full photon energy as internal vibrational excitations.

As discussed in section 2.2.1, anharmonicity, Fermi resonances, and higher-order vibrational couplings have a profound influence on the absorption spectrum of PAHs, in particular, in the CH stretching region.[8] Much of the spectral detail which is present in the low-temperature absorption

https://doi.org/10.1021/acs.jpca.2c01849
J. Phys. Chem. A 2022, 126, 3198−3209

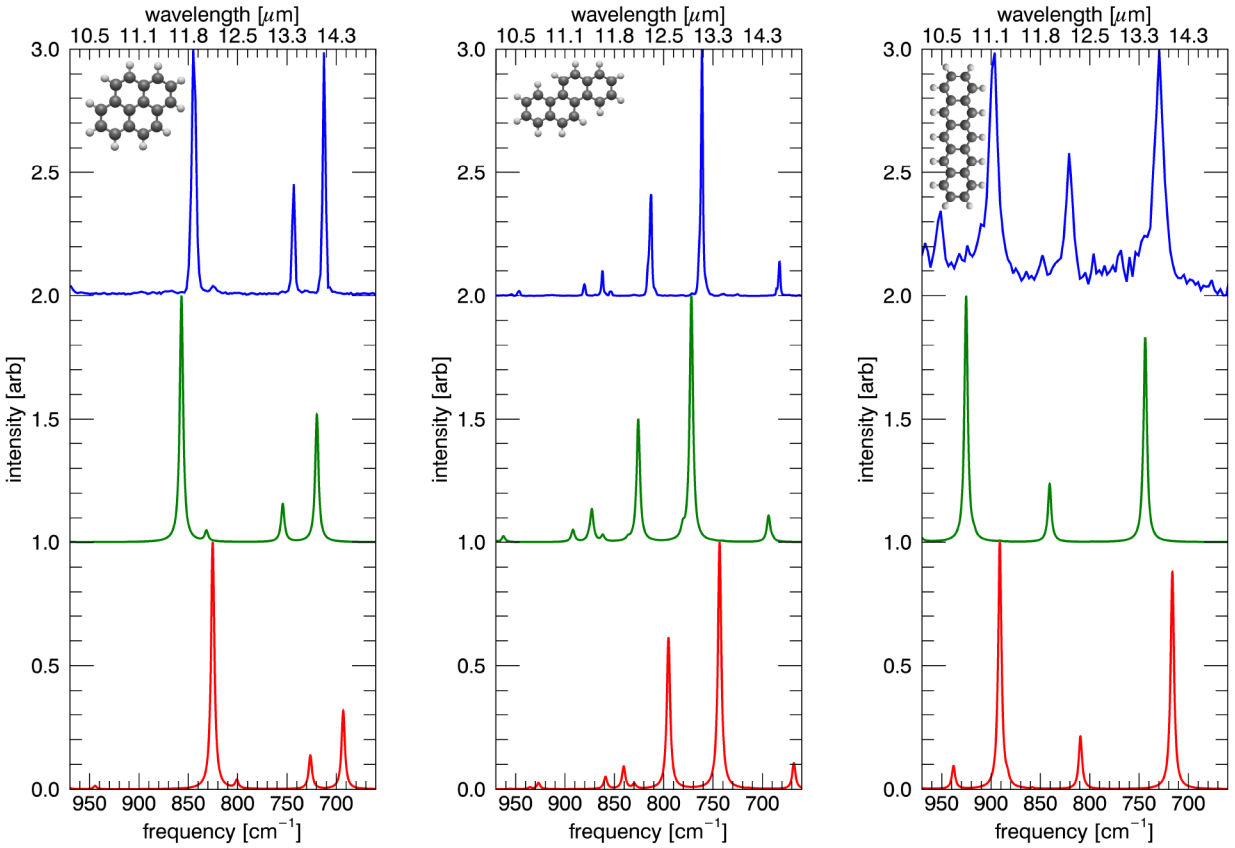

Figure 3. Absorption spectra of pyrene (left), chrysene (center), and pentacene (right) in the 11−14 μm CH out-of-plane bending-mode region. (Top) Gas-phase absorption spectra measured using an ion-dip technique (pyrene and pentacene)[11,37] and matrix isolation spectra (chrysene).[13] (Middle) Computed absorption spectra accounting for anharmonicity and resonance effects. (Bottom) Computed absorption spectra in the double-harmonic approximation, with frequencies scaled by a factor of 0.963.

spectra blends away in the emission spectrum of a highly excited PAH, leaving a broad, single peak that is shifted from the absorption position due to anharmonicity and resonance (section 3.1). As the comparison between our model and the emission experiment (Figure 2) reveals, the shifts and the broadening are well described by the theoretical model. Indeed, even the subtle shifts in peak position and profile when changing the internal energy from 5 to 7 eV are well captured by theory (Figure 2). Similar good agreement is obtained in models for the 11.2 μm band in pyrene.[36] As these comparisons demonstrate, the present theory describes the emission process and the resulting profiles at a level that is quite adequate for comparison to observations of the AIBs.

2.2.3. Laboratory Absorption Spectrum of the CH Out-of-Plane Bending Modes. The aromatic CH out-of-plane bending modes occur in the 750−920 cm^{-1} (11−14 μm) range, and the pattern of bands in this region is very characteristic of the molecular periphery of the PAH. This pattern was originally recognized for substituted benzene and naphthalene.[38,39] More recent studies have determined the correlations between the molecular structure and spectral pattern of the PAH vibrational modes.[11,40] We can recognize solo H atoms (no hydrogens on adjacent carbons), duo H atoms (two adjacent carbons each with a hydrogen atom), trio H atoms (three adjacent carbons each with a hydrogen atom), and quartet H atoms (four adjacent carbons each with a hydrogen atom). Each of these "edge" groups absorbs in well-separated frequency ranges. The precise frequency range is slightly sensitive to the charge state,[41] and for neutrals, the CH out-of-plane bending mode ranges are 860−900, 800−860, 750−810, and 730−770 cm^{-1} (11.1−11.6, 11.6−12.5, 12.4−13.3, and 13−13.6 μm) when going from solos to quartets.

Figure 3 compares the IR spectra of pyrene, chrysene, and pentacene in this wavelength range. These PAHs contain duos and trios, duos and quartets, and solos and quartets, respectively. The influence on the CH out-of-plane bending mode pattern is immediately apparent. Anharmonic calculations are in good agreement with the gaseous absorption spectra in terms of peak position and relative intensity. Harmonic calculations perform equally well after applying the 0.963 correction factor. We note that this spectral range is not much affected by resonance effects, greatly contributing to the ease of use of these patterns in species identification.

2.2.4. Intrinsic strength of the CH modes. The ratio of the intensities of the 3.3 to 11.2 μm AIBs has been used to estimate the typical size of PAHs in the interstellar PAH family.[42−47] These estimates depend, however, on the adopted intrinsic strength of the modes involved, and these are taken generally from (harmonic) calculations.

The NASA Ames PAH database (hereafter PAHdb) contains synthetic spectra of 4233 species computed in the double harmonic approximation using DFT.[6,48−50]

When comparing the intrinsic strength of the CH modes in neutral PAHs, it was noted that the calculated intrinsic strength of the CH stretching modes is overestimated by about a factor of 2 when compared to the CH out-of-plane bending mode for a

https://doi.org/10.1021/acs.jpca.2c01849
J. Phys. Chem. A 2022, 126, 3198−3209

number of small PAHs.[2,51,52] This is a very general point for CH stretching modes,[2] but it is not due to effects associated with the matrix isolation technique as previously hypothesized because this overestimation is also present when comparing the computed spectra to the gas-phase absorption spectra in the NIST database.[37] The overestimation of the intrinsic intensities can be attributed to the use of a limited basis set in the PAHdb computations, chosen as a compromise between accuracy and computational costs. Good agreement with gas-phase ratios, however, has been obtained previously when employing the N07D basis set. Figure 4 illustrates this point for a number of small PAHs. The limited comparison in Figure 4 suggests using an intrinsic strength ratio scaling of about 2 for the out-of-plane CH bending modes relative to the CH stretching modes when using harmonic calculations from the NASA Ames Database.

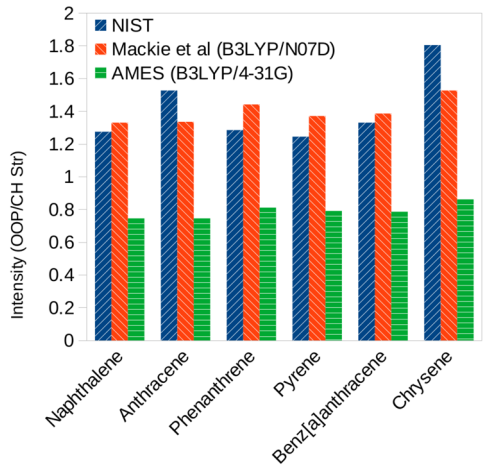

Figure 4. Ratios of the intrinsic strength of the out-of-plane CH vibrational modes (500−1000 cm^{-1}) to the CH stretching modes (3000−3250 cm^{-1}) for various PAHs. Plotted are the NIST experimental gas-phase absorption data (blue), DFT harmonic vibrational spectra using B3LYP/N07D (orange, this work), and DFT harmonic vibrational spectra using B3LYP/4-31G (green, typical of the AMES database).

3. RESULTS AND DISCUSSION

3.1. Interstellar Emission Spectrum. The detailed profile of the vibrational bands depends on the internal excitation of the emitting species. The energy cascade during the emission process will partially obscure this dependence but subtle variations remain noticeable, and this has been discussed in detail for the out-of-plane bending modes.[18] Here, we discuss this aspect for the aromatic CH stretching mode. Figure 5 shows the computed profiles for the aromatic CH stretching mode of pyrene, chrysene, and pentacene, where the full IR cascade is included in the simulation. At a low initial excitation energy, the profile for all species is quite complex with multiple peaks. These are due to resonance interactions that allow combination bands and overtones to borrow intensity from the $\nu = 1$ of the normal modes. For pyrene, as the internal excitation increases, these secondary features shift to lower energies and blend into a (weak) wing on the main band. At the same time, the peak shifts to slightly lower frequencies and the profile becomes noticeably broader. Likewise, for chrysene the distinct features blend together and shift to lower energies, albeit over a broadened range. In contrast, for pentacene, multiple peaks remain present throughout the full excitation energy range. This is a general conclusion. Highly symmetric, compact PAHs, such as pyrene, develop rather simple emission spectra in the CH stretching region, dominated by a single peak. This emission band also develops a low-frequency red-shaded wing: the telltale signature of the effects of anharmonicity in highly excited species.[18] As discussed in section 2.2.1, at low temperatures, asymmetric, noncompact PAHs show significant absorption over a wide frequency range.[9] This gives rise to multiple emission bands in the aromatic CH stretching region, which can result in a broadened CH stretching region or can even persist as distinct bands with increasing excitation (Figure 5). The red dashed curve superimposed on the top trace of each panel (8 eV cascade) in Figure 5 represents the observed emission of the AIBs in the Orion Bar.[53] As Figure 5 well illustrates, the observed profile of the 3.3 μm AIB points to the dominance of highly symmetric, compact PAHs in the interstellar PAH family.

The profile of the CH stretching mode broadens with excitation, and this is quantified in Figure 6. For symmetric compact PAHs, such as pyrene anharmonic interactions lead to a broad asymmetric, red-shaded emission profile (Figure 5). For asymmetric PAHs, the width of the CH stretching mode reflects the presence of multiple types of CH environments (cf., pentacene and chryene in Figure 5) with their specific peak positions. Each of these broadens with increasing excitation, leading to a very broad, blended profile. Finally, resonance broadening will also become more significant with increasing size as more combination bands will be involved in the resonance polyad.

3.1.1. Emission Profile. The profile of the CH out-of-plane bending modes has recently been discussed in detail.[18] Because these bands are reasonably isolated, they can be used to illustrate the effects of anharmonicity on the line profile rather well. In general, these bands show a steep blue rise and a pronounced red wing. The analysis reveals that the detailed profile is controlled mainly by three variables: the energy of the absorbed UV photon at the start of the cascade process, the size of the emitting PAH, and the rotational temperature of the PAH (which is also size-dependent). The first two variables determine the excitation (i.e., the energy per mode, $E/(3N-6)$). For typical UV photon energies (6−10 eV) and PAH sizes (50 atoms), the energy per modes ranges from 300 to 500 cm^{-1}. Hence, low-frequency modes may typically have one or two excitations, but high-frequency modes are populated only part of the time. At low temperatures, the emission spectrum is well represented by the absorption spectrum. However, as the energy per mode increases, other modes are populated and anharmonic interactions between the modes shift the emission band to lower frequencies. This shift becomes more pronounced when the excitation increases as more spectator states become populated and the population of these spectator states climbs higher on their vibrational ladder. This effect is already apparent in the frequency shift of the CH stretching mode with internal energy (Figure 2), and it is more pronounced for the relatively isolated CH out-of-plane bending modes.[18] During the radiative decay, the excited species cascade down in energy and the resulting profile centers on the low-temperature absorption peak but with a pronounced red-shaded wing.

The rotational excitation has only a minor effect. For a given excitation, it slightly broadens the emission profile. In the final cascade profile, the rotational broadening manifests itself mainly in the steepness of the blue rise of the profile.[18] For isolated molecules, the rotational excitation is set by the vibrational relaxation process. After many excitation-relaxation cycles, the

https://doi.org/10.1021/acs.jpca.2c01849
J. Phys. Chem. A 2022, 126, 3198−3209

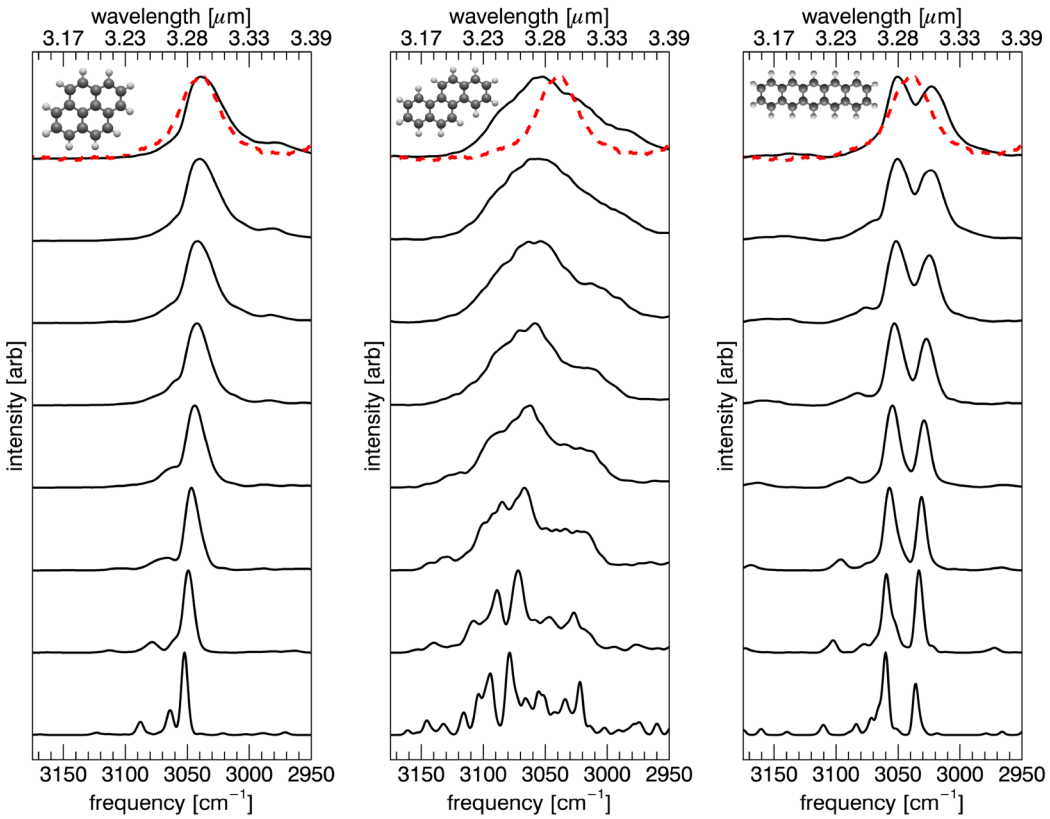

Figure 5. CH stretching region (3.3 μm) of pyrene (left), chrysene (middle), and pentacene (right) as a function of increasing initial cascade energies, from 1 eV (bottom) to 8 eV (top) in increments of 1 eV. Note that the profiles are normalized. In reality, a highly excited PAH will emit more of its internal energy in the CH stretching mode than a less-excited PAH. The dashed red spectrum at 8 eV is the observed PAH emission from the Orion Bar.[53]

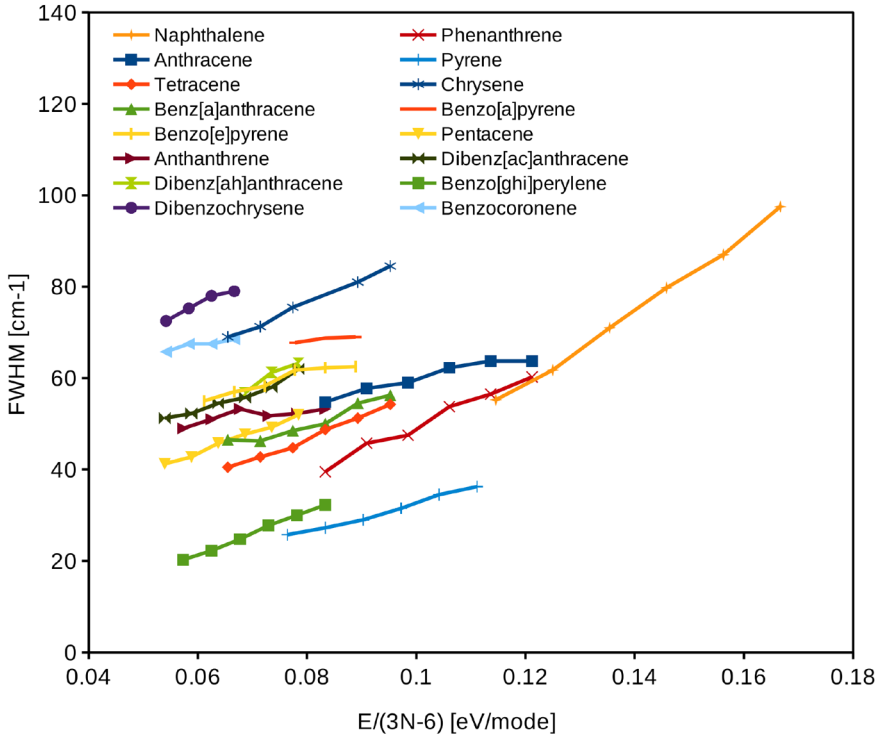

Figure 6. Full width at half-maximum (fwhm) of the CH stretching mode as a function of the initial internal excitation, $E/(3N-6)$. The profiles take the full cascade into account. The different curves represent the results of simulations for different PAHs as indicated in the legend.

https://doi.org/10.1021/acs.jpca.2c01849
J. Phys. Chem. A 2022, 126, 3198−3209

rotational population is well described by a Gaussian distribution at an effective rotational temperature given by

$$T_{\rm rot} \equiv \frac{hcBJ_{\rm ir}^{\ 2}}{k} = \frac{hc\bar{\nu}}{6k} \quad (3)$$

where B is the rotational constant, $J_{\rm ir}$ the most probable rotational quantum number, $\bar{\nu}$ the average energy of the vibrational photons emitted, and the factor 6 reflects the integration of the K ladder.[54,55] Given the low density in emission regions in space, collisional excitation has only a minor effect on the rotational population.[54,55] The broadening is then given by $\Delta\nu \simeq 4B\sqrt{kT_{\rm rot}/hcB}$ and this is about $\Delta\nu \simeq 1.6\sqrt{\bar{\nu}B} \simeq 4$ cm^{-1} for $\bar{\nu} = 1000$ cm^{-1} assuming $B = 5 \times 10^{-3}$ cm^{-1}, which is appropriate for a 30 carbon atom compact PAH. Given that the anharmonic broadening is on the order of 20−30 cm^{-1}, it is clear that rotational broadening has a relatively minor effect. Besides changing the steepness of the blue rise of the profile, rotational broadening will also lead to (blue) shifts in the apparent peak position of the feature by about $\Delta\nu$.

Figure 7 summarizes the results of cascade simulations of the CH out-of-plane bending mode as a function of internal excitation for a number of PAHs in terms of the full width at half-maximum (fwhm). Because the blue side is sensitive only to the rotational excitation, the observed increase in the fwhm with excitation reflects the effects of anharmonicity on the red-shaded profile. For the analyzed PAHs, the fwhm ranges from about 5 to 15 cm^{-1}. Besides excitation, the broadening also depends on the molecular structure involved (Figure 7). From the limited data available, anharmonic broadening seems to be more pronounced in the acene-related family than for more compact PAHs. Additional studies are required to separate the anharmonic from the molecular structure effects.

Finally, we note that the detailed profile of vibrational modes may also be affected by blending with other modes.[18]

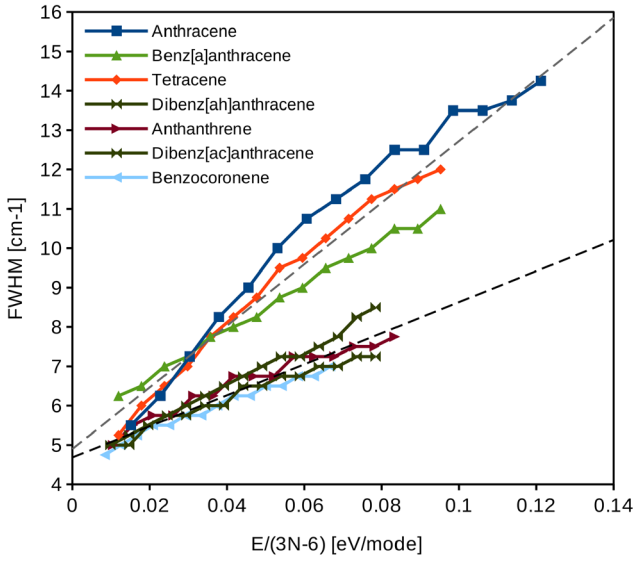

Figure 7. Full width at half-maximum (fwhm) of the CH out-of-plane bending mode as a function of the initial internal excitation $E/(3N-6)$, with N being the total number of atoms in the species. The profiles take the full cascade into account. The different curves represent the results of simulations for different PAHs as indicated in the legend. A bimodal distribution is present, so two linear fits are presented.

4. ASTROPHYSICAL IMPLICATIONS

4.1. Ratio of the CH Modes. The CH modes are the dominant vibrational relaxation channels for neutral PAHs. Given the large energy difference between the CH stretching and out-of-plane bending modes, the intensity ratio of these modes is very sensitive to the level of internal excitation. Because the available UV photon excitation energy is limited to a relatively narrow range (≃6−13.6 eV) in the interstellar medium of space, this ratio provides a convenient measure of the size of the emitting PAHs. This technique has been widely used in the size analysis of the interstellar PAH family.[42,43,45−47] Of course this ratio is sensitive to the predicted intrinsic strength ratio of the modes, and these previous analyses are based on the computed results reported in the PAHdb. As discussed in section 2.2.4, these computations have underestimated the intrinsic strength of the CH stretch by about a factor of 2, and this leads to an overestimate of the size of the emitting PAHs.

For a number of PAHs, Figure 8 shows the computed intensity ratio of the CH stretching modes to the out-of-plane bending modes as a function of excitation energy, taking the full IR cascade into account. Because the intrinsic strength ratio of these modes is very similar for all species (cf., Figure 8), the calculated ratio of the emission bands depends mainly on the internal excitation and is rather independent of the particular PAH species involved, validating the use of this ratio as a size indicator. A linear fit ($y = 4.04x - 0.0424$) provides a reasonable approximation for all species, where for a fixed internal excitation, we see variations in this ratio in the range of 10−20%.

In Figure 9, we present this ratio as a function of PAH size for different initial absorbed UV photon energies, where we have adopted the intrinsic strength ratio obtained from the linear fit of Figure 8. We note that there is a weak dependence on the molecular structure of the emitting PAHs, the origin of which awaits illumination by further studies. These theoretical results can be compared to the observed ratio of CH stretching modes

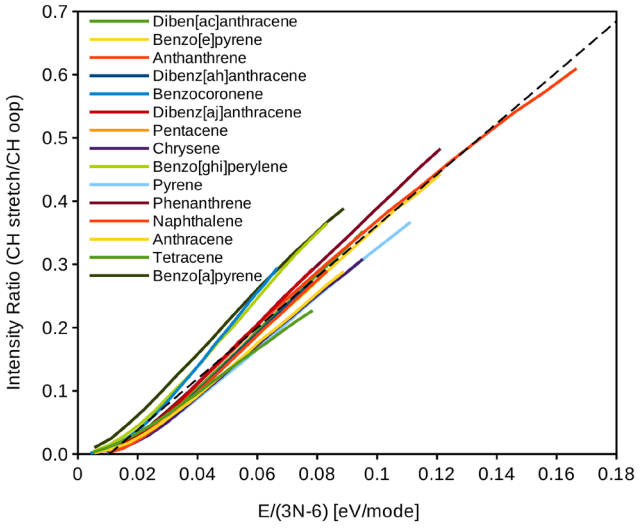

Figure 8. Computed intensity ratio of the CH stretching mode to the CH out-of-plane bending modes as a function of the initial excitation (e.g., the absorbed UV photon energy, E, divided by the number of vibrational modes, $(3N-6)$, with N being the total number of atoms in the species. These calculations take the full cascade into account. The individual curves refer to the PAH species identified in the legend. The dashed line represents the linear fit to all data.

https://doi.org/10.1021/acs.jpca.2c01849
J. Phys. Chem. A 2022, 126, 3198−3209

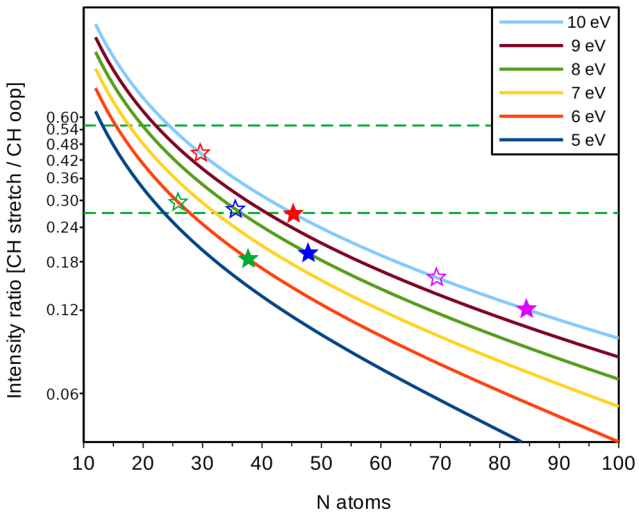

Figure 9. Computed intensity ratio of the CH stretching mode to the out-of-plane bending modes as a function of the PAH size. The different curves represent different initial absorbed UV photon energies as indicated in the legend. Solid data points correspond to the 3.3/11.2 μm AIB ratios measured by the SWS in large apertures in the Orion Bar, the reflection nebulae (NGC 7023), and the planetary nebulae (NGC 7027 and IRAS 21282 + 5050). Open data points correspond to the ratio of the 3.3/(11.2 + 12.7) AIBs measured for these sources. These data points are taken from ref 53 and plotted at the average absorbed UV photon energy typical for these sources (Orion Bar: 8 eV (blue stars); NGC 7023: 6 eV (green stars); NGC 7027: 10 eV (red stars); IRAS 21282 + 5050: 10 eV (purple stars). The two horizontal dashed green lines represent the observed systematic variation in the 3.3/11.2 AIB band ratio in the reflection nebula, NGC 7023.[45]

to the out-of-plane bending modes in the Orion Bar (a photodissociation region within NGC 1976), NGC 7023, NGC 7027, and IRAS 21282 + 5050 (Figure 9). We infer typical sizes of the emitting PAHs in these objects to be in the ranges of 35−48, 26−37, 30−45, and 69−85 atoms, respectively. In terms of the number of carbon atoms for compact PAHs, these approximate to 22−30, 16−24, 18−28, and 48−60, respectively. The presence of a size range is indicative of which specific AIBs are included in this analysis. The interstellar 11−14 μm spectrum typically shows two out-of-plane bending modes at 11.2 and at 12.7 μm. The upper estimates for the sizes quoted above assume that both of these AIBs originate from the same species, and the lower estimates assume only that the 11.2 μm mode originates from the same species. The 12.7 AIB feature, however, is observed to correlate well with the 6.2 and 7.7 μm AIBs but not with the 11.2 μm AIB. This behavior may indicate that the physical conditions that favor duos/trios over solos (section 2.2.3) also favor ionization.[41] Alternatively, this correlation behavior has been interpreted to indicate that, like the 6−9 μm modes,[53] the 12.7 μm AIB is carried by ionized PAHs.[47,56] As quantum chemistry clearly reveals, the 3.3 μm CH stretching mode can be safely attributed to (small) neutral PAHs,[53] but if the 12.7 μm AIB is due to PAH cations, then its integrated intensity should not be included in this analysis (e.g., the size of the emitting PAH should be estimated from the observed ratio of the 3.3 to the 11.2 μm AIBs). As Figure 9 demonstrates, this has quite an effect on the derived sizes. Further observational studies will be required to settle this issue. Narrow band photometric studies have revealed that the ratio of the 3.3 μm band to the 11.2 μm band varies with distance from the star across the NGC 7023 reflection nebula,[45] and this has been interpreted in terms of systematic variations in the sizes of the emitting PAHs (Figure 9). We do note, though, that these studies do not include the 12.7 μm AIB and that the 12.7/11.2 μm AIB ratio varies systematically from about 0.3 to 1.3 over this nebula, which may well influence the derived sizes if the 12.7 μm AIB is carried by neutral PAHs. The James Webb Space Telescope (JWST) can be expected to record spectra of the AIBs in a wide variety of regions and address the issue of the charge state of the 12.7 μm AIB. Figure 9 can then be used as a guide to interpret the observed ratios in terms of the size of the emitting PAHs and to relate them to (UV) processing in these regions. As this study demonstrates, ionization and size are two crucial but separate issues that are worthy of further study.

4.2. Anharmonicity and the Observed Profiles of the AIBs. The well-isolated AIBs at 5.75, 6.2, and 11.2 μm show a profile with a pronounced red-shaded wing (Figure 10).

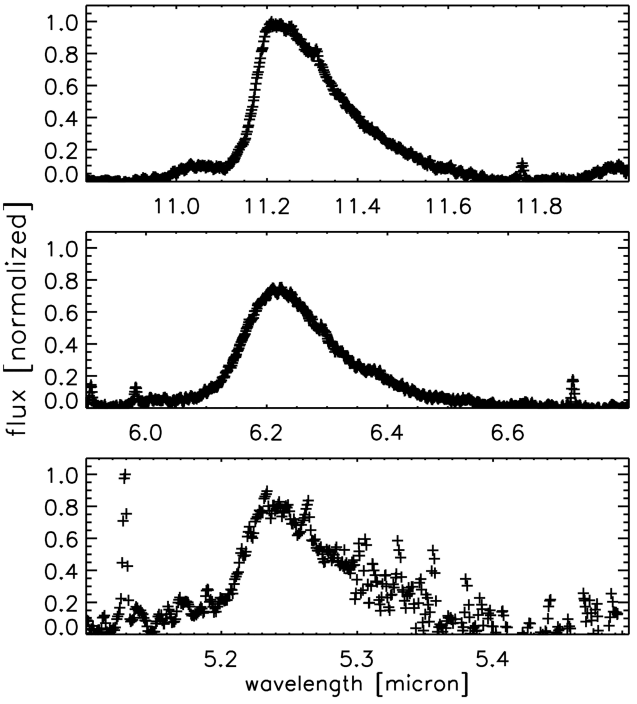

Figure 10. Observed profiles of the 11.2, 6.2, and 5.7 μm AIBs in the planetary nebula, NGC 7027, show a pronounced red-shaded wing. This figure was adapted from ref 57.

Although this wing may be due to the blending of several components contributed by different species in the interstellar PAH family with slightly different frequencies,[53] the more likely explanation is that this reflects the importance of anharmonicity.[18,59−61] Using the calculated anharmonic interaction terms, simulations of the 11.2 μm band taking the full IR cascade into account show good agreement with the observed profiles,[18] providing strong support for the interpretation of this red-shaded wing in terms of anharmonic interactions. Typically, the profiles of the AIBs show only small variations in the peak position and strength of the red-shaded wing from source to source and within individual sources.[53,58] The Orion Bar spectrum shown in the top panel of Figure 11 represents the typical 11.2 μm spectrum well, and the NGC 7027 planetary nebula shows the typical range of broadening observed in astronomical samples. The spectrum of the IRAS 21282 + 5050 planetary nebula is an exceptional spectrum with a red-shaded

https://doi.org/10.1021/acs.jpca.2c01849
J. Phys. Chem. A 2022, 126, 3198−3209

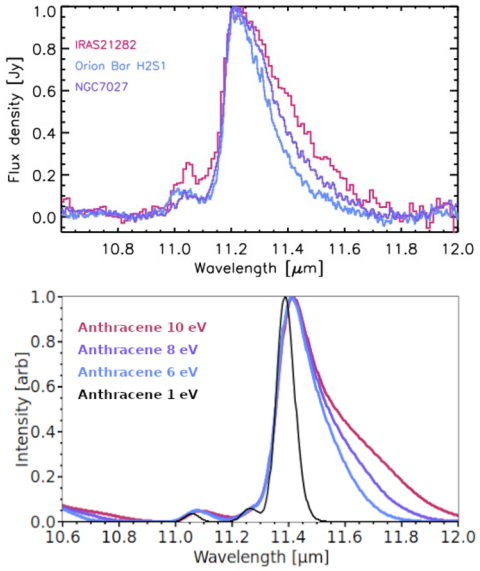

Figure 11. (Top) Observed profiles of the 11.2 μm AIB in the Orion Bar and the planetary nebulae, NGC 7027 and IRAS 21282 + 5050. This image was adapted from refs 53 and 58. (Bottom) Simulated cascade emission spectrum of anthracene at 1, 6, 8, and 10 eV. Note the change in the relative strength of the red-shaded wing in both panels as the internal energy increases.

wing that is about twice as broad as that of the Orion Bar (Figure 11).

The observed differences in the extent of the red-shaded wing of the 11.2 μm AIB can be attributed to excitation differences. The change in excitation can result either from the source of UV photons (i.e., a hotter stellar source or a higher incident far-ultraviolet (FUV) radiation field) or from a change in the PAH size (i.e., a PAH can redistribute the absorbed UV energy across more or fewer vibrational modes).[60,62] Given the similarity in the blue rise of the 11.2 μm band in these spectra and given that the peak position of this out-of-plane bending mode would shift slightly with the molecule involved, we consider that these profile variations likely reflect a difference in mainly the source of UV photons. This is illustrated in Figure 11 for the anthracene IR cascade emission at three different initial internal energies. These internal energy variations are reasonable because the Orion Bar is illuminated by an O6.5 V star and has a radiation field that is about $G_0 = 4 \times 10^4$, the average interstellar radiation field. The central star of NGC 7027 is a very hot ($\simeq$200 000 K) white dwarf with $G_0 = 6 \times 10^5$, and IRAS 21282 + 5050 has a carbon-rich Wolf-Rayet central star (WC11, $T_{\mathrm{eff}} \simeq 45\,000$ K) and $G_0 = 2 \times 10^6$.[63−67] We stress that this comparison is meant only to be an example. Indeed, the anthracene solo out-of-plane bending mode is displaced to longer wavelength as compared to the 11.2 μm AIB, illustrating that the observed red-wing strength variations in the AIB can be well matched for reasonable excitation parameters.

As a general note of caution, the 11.2 μm AIB has a weak companion band at shorter wavelength, 11.0 μm. As this band increases in intensity and develops a red-shaded profile, the profile of the 11.2 μm AIB will be distorted, and care is needed to disentangle these bands.[18]

4.3. Identification. The results presented in this article have some important ramifications for identification efforts. As Figure 5 illustrates, chrysene and pentacene show very broad and complex CH stretching mode profiles with substructure or even multiple peaks over the relevant UV photon excitation range. This is a general property for noncompact, asymmetric PAHs, which all show absorption activity in their CH stretching modes over a wide frequency range.[8,9] In contrast, the observed 3.3 μm AIB has a single peaked profile, albeit with some minor substructure present.[29,58] Hence, this class of species cannot have a high abundance in the interstellar PAH family. In contrast, the calculated cascade spectrum of the CH stretching mode in the compact PAH, pyrene, compares well to the observed profile of the 3.3 μm AIB band (red trace in Figure 5).

The dominance of highly symmetric, compact PAHs in the interstellar PAH family is supported by other lines of evidence. Specifically, the 500−650 cm^{-1} (15−20 μm) spectral range represents the transition from bands due to pure group molecular vibrations to bands involving larger parts of the PAH skeleton (i.e., the C−C−C deformation modes). Quantum chemical studies of irregular PAHs reveal very complex spectra, generally with many bands; in contrast, highly symmetric, compact PAHs have very simple spectra with typically one dominant band.[28,44] Because the observed AIB spectrum reveals the presence of only a few well-defined bands,[68] highly symmetric, compact PAHs seem to dominate the interstellar PAH family. The 1250−1300 cm^{-1} (7 to 8 μm) range is equally revealing. The observed AIB spectrum is rather simple, with major bands at 7.6, 7.8, and 8.6 μm, though there is some weak spectral structure present at high spectral resolution.[69] Irregular, asymmetric PAHs have many active modes in the frequency range, while the spectra of symmetric, compact PAHs are dominated by a few bands.[28,44,70,71]

Finally, we draw attention to Figure 11. The blue rise of the observed 11.2 μm AIB is similar in all three sources. Experiments and theory show small variations in the peak position of the solo CH out-of-plane bending mode at the 5 to 10 cm^{-1} (0.1 μm) level within the (limited) subset of PAHs studied.[11,72] Such variations would show up as shifts in the blue rise and peak position of this AIB. Studies on a larger set of relevant PAHs will have to confirm this, but for now we tentatively conclude that the same species are responsible for the AIB emission in these three very different sources, which supports the suggestion that the interstellar PAH family is dominated by a few very stable PAHs, the so-called grandPAHs.[73,74]

5. CONCLUSIONS

In support of the analysis of the AIBs in interstellar spectra, we have studied in detail the characteristics of the CH stretching and out-of-plane bending modes in neutral PAHs. We have calculated the low-temperature absorption spectra using anharmonic DFT, taking resonances into account. This method has been validated against laboratory spectra of a set of (small) PAHs. We have applied a model for the infrared cascade that occurs when a UV-excited PAH relaxes through vibrational emission, and we have used this to calculate the expected profile of the emission bands. These model spectra can be compared in detail to spectra observed in space.

Our detailed conclusions are as follows:

1. Anharmonic interactions, including mode couplings, perturbations, and resonance effects, lead to large (relative to harmonic) frequency shifts, the inclusion of which is necessary to bring theory into agreement with experimental spectra, especially in the CH stretching region. For spectra calculated with the double-harmonic approximation using B3LYP/4-31G, this is typically

https://doi.org/10.1021/acs.jpca.2c01849
J. Phys. Chem. A 2022, 126, 3198−3209

compensated for by a frequency-dependent correction factor. However, anharmonic theory using B3LYP/N07D is in good (0.5%) agreement with experimental peak positions without the need for a scaling factor.

2. Besides anharmonic shifts in frequency, the CH stretching modes are greatly affected by resonance interactions. The anharmonic theoretical spectra are in excellent agreement with the experimental spectra in terms of the frequency range and relative strength of the modes. In particular, the redistribution of intensity from the intrinsically bright modes to the weak or normally dark transitions is important. While anharmonicities affect the position and profile of the CH out-of-plane bending modes, resonances are found to be less important for these modes.
3. In agreement with previous studies,[2,37] we conclude that the relative strength of the CH stretching modes with respect to the CH out-of-plane bending modes is overestimated in the spectra collected in the PAHdb. This reflects the limited basis set, driven by computational cost considerations, used in the calculation of these spectra. Good agreement with experiments is obtained for anharmonic calculations using the B3LYP/N07D functional/basis set. We have recalibrated the widely employed relationship between the observed relative strength of these modes in astronomical spectra and the size of the emitting PAHs in Figure 9. We conclude that species in the interstellar PAH family are typically 16−30 carbon atoms, depending on the region, and this contrasts with previous estimates ranging from 35−80 to 50−105 carbon atoms.[45] If confirmed, this will represents a dramatic change in the understanding of the interstellar PAH population.
4. The calculated emission profiles of the CH stretching mode in highly vibrationally excited naphthalene are in good agreement with laboratory studies in terms of peak position, red wing, and the frequency shift with excitation level, providing general support for our theoretical models.
5. The IR emission of CH stretching modes in asymmetric, noncompact PAHs shows infrared activity over a wide frequency range. This characteristic is retained after allowing for the IR cascade processes and is at odds with the observed interstellar spectra. We conclude that the 3.3 μm AIB is dominated by emission from compact PAHs.
6. The energy cascade inherent in the vibrational relaxation of isolated molecules produces red-shaded wings on their emission profiles, which is very pronounced for the CH out-of-plane bending mode. We have computed the line profile of this mode and demonstrated that the observed variations in the strength of this red-shaded wing on the 11.2 μm AIB can be well reproduced for reasonable variations in the internal excitation of the emitting species.

Experimental and theoretical spectra of small PAHs agree well in detail. Further experimental and theoretical studies are required to determine the applicability of these results to larger PAHs, PAH cations, and wider structural variety relevant to interstellar observations. Laboratory studies on millimeter-wave spectroscopy can provide insight into the pure rotational properties of PAHs that enter into these calculations. In addition, such studies can guide astronomical searches for the rotational transitions of PAHs that can be used as fingerprints for identification purposes. Theoretical studies will require either an increase in computer power or clever algorithms that link anharmonicity for similar modes to the size and structure of the species involved. JWST can be expected to observe interstellar PAH spectra at high sensitivity and spectral resolution in a wide variety of environments. Models such as those presented here will be instrumental in linking the observed spectral characteristics to the inherent molecular properties of the species in space.

AUTHOR INFORMATION

Corresponding Author

Cameron J. Mackie − *Kenneth S. Pitzer Center for Theoretical Chemistry, Department of Chemistry, University of California, Berkeley, California 94720, United States; Chemical Sciences Division, Lawrence Berkeley National Laboratory, Berkeley, California 94720, United States;* orcid.org/0000-0003-2885-2021; Email: mackie@lbl.gov

Authors

Alessandra Candian − *van 't Hoff Institute for Molecular Science, University of Amsterdam, 1090 GD Amsterdam, The Netherlands;* orcid.org/0000-0002-5431-4449

Timothy J. Lee − *NASA Ames Research Center, Moffett Field, California 94035-1000, United States;* orcid.org/0000-0002-2598-2237

Alexander G. G. M. Tielens − *Leiden Observatory, Leiden University, 2300 RA Leiden, The Netherlands; Astronomy Department, University of Maryland, College Park, Maryland 20742, United States*

Complete contact information is available at: https://pubs.acs.org/10.1021/acs.jpca.2c01849

Notes

The authors declare no competing financial interest.

ACKNOWLEDGMENTS

T.J.L. gratefully acknowledges support from NASA grants 17-APRA17-0051, 18-APRA18-0013, 18-XRP18-2-0029, and NNH20ZDA001N-EW. Research on interstellar PAHs at Leiden Observatory is supported through a Spinoza Award from the Dutch Science Organization (NWO). We are grateful to Prof. Els Peeters for retrieving the ISO/SWS spectra used here.

REFERENCES

(1) Tielens, A. G. G. M. Interstellar polycyclic aromatic hydrocarbon molecules. *Annu. Rev. Astron. Astrophys.* **2008**, *46*, 289−337.

(2) Bauschlicher, C. W.; Langhoff, S. R. The calculation of accurate harmonic frequencies of large molecules: The polycyclic aromatic hydrocarbons, a case study. *Spectrochim. Acta, Part A* **1997**, *53*, 1225−1240.

(3) Bauschlicher, C. W.; Ricca, A.; Boersma, C.; Allamandola, L. J. The NASA Ames PAH IR Spectroscopic Database: Computational Version 3.00 with Updated Content and the Introduction of Multiple Scaling Factors. *Astrophys. J., Suppl. Ser.* **2018**, *234*, 32.

(4) Jacox, M. The spectroscopy of molecular reaction intermediates trapped in the solid rare gases. *Chem. Phys. Rev.* **2002**, *31*, 108−115.

(5) Pathak, A.; Rastogi, S. Modeling the interstellar aromatic infrared bands with co-added spectra of PAHs. *Astron. Astrophys.* **2008**, *485*, 735−742.

(6) Bauschlicher, C. W.; Ricca, A. On the calculation of the vibrational frequencies of polycyclic aromatic hydrocarbons. *Mol. Phys.* **2010**, *108*, 2647−2654.

(7) Boersma, C.; Bauschlicher, J. C. W.; Ricca, A.; Mattioda, A. L.; Cami, J.; Peeters, E.; Sánchez de Armas, F.; Puerta Saborido, G.;

Hudgins, D. M.; Allamandola, L. J. The NASA Ames PAH IR Spectroscopic Database Version 2.00: Updated Content, Web Site, and On(Off)line Tools. *Astrophys. J., Suppl. Ser.* **2014**, *211*, 8.
(8) Maltseva, E.; Petrignani, A.; Candian, A.; Mackie, C. J.; Huang, X.; Lee, T. J.; Tielens, A. G. G. M.; Oomens, J.; Buma, W. J. High-resolution IR Absorption Spectroscopy of Polycyclic Aromatic Hydrocarbons: The Realm of Anharmonicity. *Astrophys. J.* **2015**, *814*, 23.
(9) Maltseva, E.; Petrignani, A.; Candian, A.; Mackie, C. J.; Huang, X.; Lee, T. J.; Tielens, A. G. G. M.; Oomens, J.; Buma, W. J. High-resolution IR Absorption Spectroscopy of Polycyclic Aromatic Hydrocarbons in the 3 μm Region: Role of Periphery. *Astrophys. J.* **2016**, *831*, 58.
(10) Maltseva, E.; Petrignani, A.; Candian, A.; Mackie, C. J.; Huang, X.; Lee, T. J.; Tielens, A. G. G. M.; Oomens, J.; Buma, W. J. High-resolution IR absorption spectroscopy of polycyclic aromatic hydrocarbons in the 3 μm region: role of hydrogenation and alkylation. *Astron. Astrophys.* **2018**, *610*, A65.
(11) Lemmens, A. K.; Rap, D. B.; Thunnissen, J. M. M.; Mackie, C. J.; Candian, A.; Tielens, A. G. G. M.; Rijs, A. M.; Buma, W. J. Anharmonicity in the mid-infrared spectra of polycyclic aromatic hydrocarbons: molecular beam spectroscopy and calculations. *Astron. Astrophys.* **2019**, *628*, A130.
(12) Mackie, C. J.; Candian, A.; Huang, X.; Maltseva, E.; Petrignani, A.; Oomens, J.; Buma, W. J.; Lee, T. J.; Tielens, A. G. G. M. The anharmonic quartic force field infrared spectra of three polycyclic aromatic hydrocarbons: Naphthalene, anthracene, and tetracene. *J. Chem. Phys.* **2015**, *143*, 224314.
(13) Mackie, C. J.; Candian, A.; Huang, X.; Maltseva, E.; Petrignani, A.; Oomens, J.; Mattioda, A. L.; Buma, W. J.; Lee, T. J.; Tielens, A. G. G. M. The anharmonic quartic force field infrared spectra of five non-linear polycyclic aromatic hydrocarbons: Benz[a]anthracene, chrysene, phenanthrene, pyrene, and triphenylene. *J. Chem. Phys.* **2016**, *145*, 084313.
(14) Mackie, C. J.; Candian, A.; Huang, X.; Maltseva, E.; Petrignani, A.; Oomens, J.; Buma, W. J.; Lee, T. J.; Tielens, A. G. G. M. The anharmonic quartic force field infrared spectra of hydrogenated and methylated PAHs. *Phys. Chem. Chem. Phys.* **2018**, *20*, 1189−1197.
(15) Basire, M.; Parneix, P.; Calvo, F.; Pino, T.; Bréchignac, P. Temperature and anharmonic effects on the infrared absorption spectrum from a quantum statistical approach: Application to naphthalene. *J. Phys. Chem. A* **2009**, *113*, 6947−6954.
(16) Basire, M.; Parneix, P.; Pino, T.; Bréchignac, Ph.; Calvo, F. Modeling the anharmonic infrared Emission Spectra of PAHs: Application to the Pyrene Cation. *EAS Publications Series* **2011**, *46*, 95−101.
(17) Mackie, C. J.; Chen, T.; Candian, A.; Lee, T. J.; Tielens, A. G. G. M. Fully anharmonic infrared cascade spectra of polycyclic aromatic hydrocarbons. *J. Chem. Phys.* **2018**, *149*, 134302.
(18) Mackie, C. J.; Candian, A.; Lee, T. J.; Tielens, A. G. G. M. Modeling the infrared cascade spectra of small PAHs: the 11.2μm band. *Theor. Chem. Acc.* **2021**, *140*, 148.
(19) Mulas, G.; Falvo, C.; Cassam-Chenaï, P.; Joblin, C. Anharmonic vibrational spectroscopy of polycyclic aromatic hydrocarbons (PAHs). *J. Chem. Phys.* **2018**, *149*, 144102.
(20) Hoy, A. R.; Mills, I. M.; Strey, G. Anharmonic force constant calculations. *Mol. Phys.* **1972**, *24*, 1265−1290.
(21) Wang, F.; Landau, D. P. Efficient, Multiple-Range Random Walk Algorithm to Calculate the Density of States. *Phys. Rev. Lett.* **2001**, *86*, 2050−2053.
(22) Frisch, M. J.; Trucks, G. W.; Schlegel, H. B.; Scuseria, G. E.; Robb, M. A.; Cheeseman, J. R.; Scalmani, G.; Barone, V.; Petersson, G. A.; Nakatsuji, H. et al. *Gaussian 16*, Revision C.01; Gaussian Inc.: Wallingford, CT, 2016.
(23) Lee, C.; Yang, W.; Parr, R. G. Development of the Colle-Salvetti correlation-energy formula into a functional of the electron density. *Phys. Rev. B* **1988**, *37*, 785.
(24) Becke, A. D. Density functional thermochemistry. III. The role of exact exchange. *J. Chem. Phys.* **1993**, *98*, 5648.
(25) Barone, V.; Cimino, P.; Stendardo, E. Development and Validation of the B3LYP/N07D Computational Model for Structural Parameter and Magnetic Tensors of Large Free Radicals. *J. Chem. Theory Comput* **2008**, *4*, 751−764.
(26) Gaw, J. F.; Willets, A.; Green, W. H.; Handy, N. C. In *Advances in Molecular Vibrations and Collision Dynamics*; Bowman, J. M., Ratner, M. A., Eds.; JAI Press, Inc.: Greenwich, CT, 1991; pp 170−185.
(27) Martin, J. M.; Taylor, P. R. Accurate ab initio quartic force field for trans-HNNH and treatment of resonance polyads. *Spectrochim. Acta, Part A* **1997**, *53*, 1039−1050.
(28) Bauschlicher, J.; Charles, W.; Peeters, E.; Allamandola, L. J. The infrared spectra of very large irregular polycyclic aromatic hydrocarbons (PAHs): Observational probes of astronomical PAH geometry, size, and charge. *Astrophys. J.* **2009**, *697*, 311−327.
(29) Candian, A.; Kerr, T. H.; Song, I. O.; McCombie, J.; Sarre, P. J. Spatial distribution and interpretation of the 3.3 μm PAH emission band of the Red Rectangle. *Mon. Not. R. Astron. Soc.* **2012**, *426*, 389−397.
(30) Cook, D. J.; Schlemmer, S.; Balucani, N.; Wagner, D. R.; Harrison, J. A.; Steiner, B.; Saykally, R. J. Single Photon Infrared Emission Spectroscopy: A Study of IR Emission from UV Laser Excited PAHs between 3 and 15 μm. *J. Phys. Chem. A* **1998**, *102*, 1465−1481.
(31) Kohn, A. W.; Lin, Z.; Van Voorhis, T. Toward Prediction of Nonradiative Decay Pathways in Organic Compounds I: The Case of Naphthalene Quantum Yields. *J. Phys. Chem. C* **2019**, *123*, 15394−15402.
(32) Siebrand, W. Radiationless Transitions in Polyatomic Molecules. I. Calculation of Franck—Condon Factors. *J. Chem. Phys.* **1967**, *46*, 440−447.
(33) Pino, T.; Carpentier, Y.; Féraud, G.; Friha, H.; Kokkin, D. L.; Troy, T. P.; Chalyavi, N.; Bréchignac, P.; Schmidt, T. W. *Electronic Spectroscopy of PAHs*; EAS Publications Series, 2011; pp 355−371.
(34) Reylé, C.; Bréchignac, P. Fluorescence of jet-cooled naphthalene: Emission spectra, lifetimes and quantum yields. *Eur. Phys. J. D* **2000**, *8*, 205−210.
(35) Kobayashi, A.; Suzuki, K.; Yoshihara, T.; Tobita, S. Absolute Measurements of Photoluminescence Quantum Yields of 1-Halonaphthalenes in 77 K Rigid Solution Using an Integrating Sphere Instrument. *Chem. Lett.* **2010**, *39*, 282−283.
(36) Chen, T.; Mackie, C.; Candian, A.; Lee, T. J.; Tielens, A. G. G. M. Anharmonicity and the infrared emission spectrum of highly excited polycyclic aromatic hydrocarbons. *Astron. Astrophys.* **2018**, *618*, A49.
(37) Lemmens, A. K. Polycyclic aromatic hydrocarbons: laboratory infrared signatures of astrochemical evolution. *Ph.D. Thesis*, 2022.
(38) Bellamy, L. J. *The Infrared Spectra of Complex Molecules*, 3rd ed.; Chapman and Hall Ltd., 1975.
(39) Socrates, G. *Infrared Characteristic Group Frequencies*; Wiley and Sons, 1980.
(40) Hudgins, D. M.; Allamandola, L. J. Interstellar PAH Emission in the 11−14 Micron Region: New Insightsfrom Laboratory Data and a Tracer of Ionized PAHS. *Astrophys. J. Lett.* **1999**, *516*, L41−L44.
(41) Hony, S.; Van Kerckhoven, C.; Peeters, E.; Tielens, A. G. G. M.; Hudgins, D. M.; Allamandola, L. J. The CH out-of-plane bending modes of PAH molecules in astrophysical environments. *Astron. Astrophys.* **2001**, *370*, 1030−1043.
(42) Allamandola, L. J.; Tielens, A. G. G. M.; Barker, J. R. Polycyclic aromatic hydrocarbons and the unidentified infrared emission bands: auto exhaust along the milky way. *Astrophys. J.* **1985**, *290*, L25−L28.
(43) Allamandola, L. J.; Tielens, A. G. G. M.; Barker, J. R. Interstellar polycyclic aromatic hydrocarbons - The infrared emission bands, the excitation/emission mechanism, and the astrophysical implications. *Astrophys. J., Suppl. Ser.* **1989**, *71*, 733.
(44) Ricca, A.; Bauschlicher, J.; Charles, W.; Boersma, C.; Tielens, A. G. G. M.; Allamandola, L. J. The Infrared Spectroscopy of Compact Polycyclic Aromatic Hydrocarbons Containing up to 384 Carbons. *Astrophys. J.* **2012**, *754*, 75.
(45) Croiset, B. A.; Candian, A.; Berné, O.; Tielens, A. G. G. M. Mapping PAH sizes in NGC 7023 with SOFIA. *Astron. Astrophys.* **2016**, *590*, A26.

https://doi.org/10.1021/acs.jpca.2c01849
J. Phys. Chem. A 2022, 126, 3198−3209

(46) Knight, C.; Peeters, E.; Stock, D. J.; Vacca, W. D.; Tielens, A. G. G. M. Tracing PAH Size in Prominent Nearby Mid-Infrared Environments. *Astrophys. J.* **2021**, *918*, 8.
(47) Maragkoudakis, A.; Peeters, E.; Ricca, A. Probing the size and charge of polycyclic aromatic hydrocarbons. *Mon. Not. R. Astron. Soc.* **2020**, *494*, 642−664.
(48) Bauschlicher, C. W., Jr.; Peeters, E.; Allamandola, L. J. The infrared spectra of very large, compact, highly symmetric, polycyclic aromatic hydrocarbons (PAHs). *Astrophys. J.* **2008**, *678*, 316−327.
(49) Boersma, C.; Rubin, R. H.; Allamandola, L. J. Spatial Analysis of the Polycyclic Aromatic Hydrocarbon Features Southeast of the Orion Bar. *Astrophys. J.* **2012**, *753*, 168.
(50) Mattioda, A.; Hudgins, D.; Boersma, C.; Bauschlicher, C.; Ricca, A.; Cami, J.; Peeters, E.; de Armas, F. S.; Saborido, G. P.; Allamandola, L. The NASA Ames PAH IR Spectroscopic Database: The Laboratory Spectra. *Astrophysical Journal Supplement Series* **2020**, *251*, 22.
(51) Langhoff, S. Theoretical infrared spectra for polycyclic aromatic hydrocarbon neutrals, Cations, and Anions. *J. Phys. Chem.* **1996**, *100*, 2819−2841.
(52) Hudgins, D. M.; Bauschlicher, J.; Charles, W.; Allamandola, L. J. Closed-shell polycyclic aromatic hydrocarbon cations: a new category of interstellar polycyclic aromatic hydrocarbons. *Spectrochim. Acta* **2001**, *57*, 907−930.
(53) Peeters, E.; Hony, S.; Van Kerckhoven, C.; Tielens, A. G. G. M.; Allamandola, L. J.; Hudgins, D. M.; Bauschlicher, C. W. The rich 6 to 9 μm spectrum of interstellar PAHs. *Astron. Astrophys.* **2002**, *390*, 1089−1113.
(54) Rouan, D.; Leger, A.; Omont, A.; Giard, M. Physics of the rotation of a PAH molecule in interstellar environments. *Astron. Astrophys.* **1992**, *253*, 498−514.
(55) Tielens, A. G. G. M. *Molecular Astrophysics*; Cambridge University Press, 2021.
(56) Boersma, C.; Bregman, J.; Allamandola, L. J. Properties of Polycyclic Aromatic Hydrocarbons in the Northwest Photon Dominated Region of NGC 7023. III. Quantifying the Traditional Proxy for PAH Charge and Assessing its Role. *Astrophys. J.* **2015**, *806*, 121.
(57) Boersma, C.; Mattioda, A. L.; Bauschlicher, J. C. W.; Peeters, E.; Tielens, A. G. G. M.; Allamandola, L. J. The 5.25 and 5.7 μm Astronomical Polycyclic Aromatic Hydrocarbon Emission Features. *Astrophys. J.* **2009**, *690*, 1208−1221.
(58) van Diedenhoven, B.; Peeters, E.; Van Kerckhoven, C.; Hony, S.; Hudgins, D. M.; Allamandola, L. J.; Tielens, A. G. G. M. The Profiles of the 3−12 Micron Polycyclic Aromatic Hydrocarbon Features. *Astrophys. J.* **2004**, *611*, 928−939.
(59) Barker, J. R.; Allamandola, L. J.; Tielens, A. G. G. M. Anharmonicity and the interstellar polycyclic aromatic hydrocarbon infrared emission spectrum. *Astrophys. J.* **1987**, *315*, L61.
(60) Pech, C.; Joblin, C.; Boissel, P. The profiles of the aromatic infrared bands explained with molecular carriers. *Astron. Astrophys.* **2002**, *388*, 639−651.
(61) Cook, D. J.; Saykally, R. J. Simulated Infrared Emission Spectra of Highly Excited Polyatomic Molecules: A Detailed Model of the PAH-UIR Hypothesis. *Astrophys. J.* **1998**, *493*, 793−802.
(62) Candian, A.; Sarre, P. J. The 11.2 μm emission of PAHs in astrophysical objects. *Mon. Not. R. Astron. Soc.* **2015**, *448*, 2960−2970.
(63) Balega, Y. Y.; Chentsov, E. L.; Rzaev, A. K.; Weigelt, G. Physical Properties of the Massive Magnetic Binary θ^1 Ori C Components. *Physics and Evolution of Magnetic and Related Stars*; ASP Conference Proceedings, Nizhny Arkhyz, Russia, Aug 25−31, 2015; Vol. *494*, p 57.
(64) Bieging, J. H.; Boley, P. A.; Latter, W. B.; Tielens, A. G. G. M. A Search for Temperature and Density Variations in NGC 7027 with the Hubble Space Telescope. *Astrophys. J.* **2008**, *676*, 390−401.
(65) Cohen, M.; Jones, B. F. Optical Spectroscopy of IRAS Sources with Infrared Emission Bands: IRAS 21282 + 5050 and the Diffuse Interstellar Bands. *Astrophys. Jl* **1987**, *321*, L151.
(66) Sander, A.; Hamann, W. R.; Todt, H. The Galactic WC stars. Stellar parameters from spectral analyses indicate a new evolutionary sequence. *Astron. Astrophys.* **2012**, *540*, A144.
(67) Tielens, A. G. G. M. *Physics and Chemistry of the Interstellar Medium*; Cambridge University Press, 2005.
(68) Boersma, C.; Bauschlicher, C. W.; Allamandola, L. J.; Ricca, A.; Peeters, E.; Tielens, A. G. G. M. The 15−20 μm PAH emission features: probes of individual PAHs? *Astron. Astrophys.* **2010**, *511*, A32.
(69) Moutou, C.; Sellgren, K.; Verstraete, L.; Léger, A. Upper limit on C_{60} and $C_{60}(+)$ features in the ISO-SWS spectrum of the reflection nebula NGC 7023. *Astron. Astrophys.* **1999**, *347*, 949−956.
(70) Bouwman, J.; Castellanos, P.; Bulak, M.; Terwisscha van Scheltinga, J.; Cami, J.; Linnartz, H.; Tielens, A. G. G. M. Effect of molecular structure on the infrared signatures of astronomically relevant PAHs. *Astron. Astrophys.* **2019**, *621*, A80.
(71) Bouwman, J.; Linnartz, H.; Tielens, A. G. G. M. Mid-infrared spectroscopic signatures of dibenzopyrene cations - The effect of symmetry on PAH IR spectroscopy. *J. Mol. Spectrosc.* **2021**, *378*, 111458.
(72) Lemmens, A. K.; Rijs, A. M.; Buma, W. J. Infrared Spectroscopy of Jet-cooled "GrandPAHs" in the 3−100 μm Region. *Astrophys. J.* **2021**, *923*, 238.
(73) Andrews, H.; Boersma, C.; Werner, M. W.; Livingston, J.; Allamandola, L. J.; Tielens, A. G. G. M. PAH emission at the bright locations of PDRs: The GrandPAH hypothesis. *Astrophys. J.* **2015**, *807*, 99.
(74) Tielens, A. G. G. M. The molecular universe. *Rev. Mod. Phys.* **2013**, *85*, 1021−1081.

https://doi.org/10.1021/acs.jpca.2c01849
J. Phys. Chem. A 2022, 126, 3198−3209